Supplementary Information (SI) for Journal of Materials Chemistry A.

Electronic Supporting Information

Synthesis of Highly Durable and Efficient Ir-Functionalized OAPS-GMA Dendrimer for All-pH Hydrogen Evolution Reaction

Amir Said,[a] Binbin Qian,[a,b,c] Ruiqian Zhang,[a] Chunlei Yang,[a] Ke Xu[a,b,c], Kunfeng Chen,[d] and Dongfeng Xue[a,b,c,*]

[a.] *Shenzhen Institute of Advanced Technology, Chinese Academy of Sciences, Shenzhen 518055, China*

[b.] *Shenzhen Institute of Advanced Technology, Shenzhen 518055, China*

[c.] *Shenzhen Institute for Advanced Study, University of Electronic Science and Technology of China, Shenzhen 518110, China*

[d.] *Institute of Novel Semiconductors, State Key Laboratory of Crystal Materials, Shandong University, Jinan 25100, China*

Corresponding author email: dfxue@uestc.edu.cn

1. Experimental Section

1.1. Materials and Chemicals

Iridium acetate ($Ir(Ac)_3$, > 98%), glycidyl methacrylate (GMA, > 98.5%), octa(phenyl)silsesquioxane (OPS, > 98%), potassium hydroxide (KOH, > 99.9%), ethylene glycol (EG, > 99.5%), hydrazine hydrate (HH, > 99%), sodium sulfate (Na_2SO_4, > 99.9 %), n-hexane (98%), fuming nitric acid (HNO_3, > 86%), ethyl acetate (EA, > 99%), absolute ethanol (EtOH, > 99.9%), acetone (C_3H_6O, > 99.5%), dimethyl formaldehyde (DMF, > 99%), petroleum ether (C_6H_{14}, > 98%), tetrahydrofuran (THF, > 99%), and sulfuric acid (H_2SO_4, > 99.08%) were ordered from Shanghai Aladdin Company (China). Nafion solution (5 wt.%) and phosphate-buffered saline (PBS) were obtained from Sigma Aldrich. Commercial platinum carbon powder (20% Pt/C) was acquired from Johson Matthey Chemicals Ltd. (Shanghai, China). The carbon paper (CP) was ordered from Toray Industries (China) Co., Ltd. Nickel foam (NF), with a thickness of 1.6 mm and a porosity of approximately 95%, was provided by Suzhou Jiashide Metal Foam Co., Ltd. All the reagents were of analytical grade and were used as received. Ultrapure water (Millipore, > 18 MΩ·cm) was used throughout the experiment.

1.2. Synthesis of Octa(aminophenyl)silsesquioxane (OAPS)

OAPS was synthesized using a two-step method (Fig. S1).

1st step: Initially, OPS (5 g, 4.9 mmol) was added in a round bottom flask, followed by the addition of 30 mL of fuming nitric acid while maintaining the temperature below 0 °C. The mixture was stirred for 60 min at this temperature, after which it was allowed to stir at room temperature for 24 h. Once the reaction was complete, the mixture was poured onto 80 g of ice to precipitate the product. The precipitate was collected by filtration and rinsed several times with water until the pH reached 6. The resultant material was further washed three times with absolute EtOH. The obtained yellow product was vacuum-dried at 45 °C, a 91% yield of ONPS.

2nd step: Poured (2.5 g, 1.93 mmol) of ONPS in a two-neck round bottom flask along with 2 g of activated charcoal, 25 mg of $FeCl_3$ (0.154 mmol), and 20 mL of dried THF. The reaction flask was equipped with a stirrer and condenser, and the mixture was stirred at 60 °C under nitrogen atmosphere (N_2 atm) for 30 min. Then, 15 mL of hydrazine hydrate was gradually added dropwise to the solution and stirred for 24 h further at room temperature. After the reaction, the solution cooled down, and 10 mL of ethyl acetate was added. The charcoal was removed by filtration, and the resulting solution was transferred to a separating funnel and rinsed several times with water. The organic phase was separated and dried by adding Na_2SO_4, then filtered and concentrated. The product was then precipitated in 400 mL n-hexane. The residues were dissolved in ethyl acetate and THF to further purify and then reprecipitated in 300 mL of n-hexane. Finally, the product was vacuum dried at 45 °C, a 75% yield of OAPS.

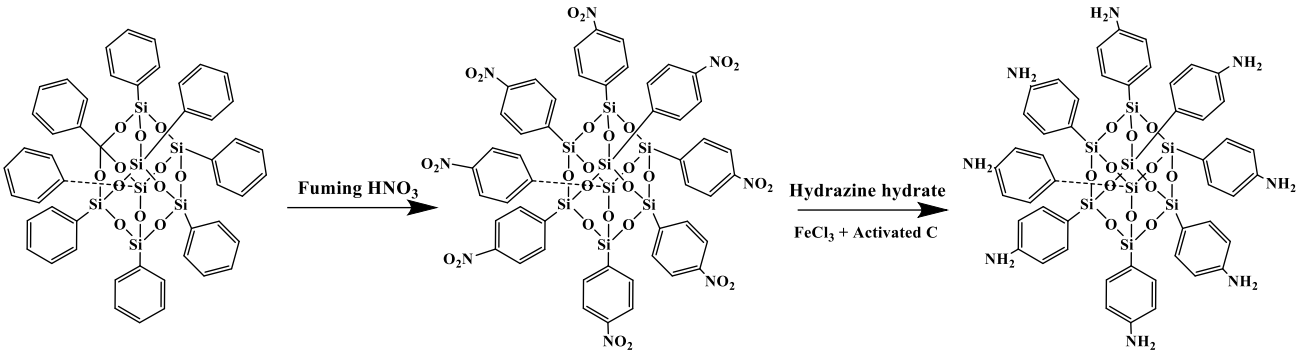

Fig. S1 Schematic representation of the synthesized OAPS.

1.3. Structural Characterizations

The samples were characterized using a Bruker D8 Advanced X-ray diffraction (XRD) system equipped with Cu Kα radiation in a range of θ = 10 to 90°. Scanning electron microscopy (SEM) images and EDX mapping were obtained using a field emission scanning electron microscope (JSM-6330F, JEOL Co LTD., Japan) operating at an accelerating voltage of 10 kV. The microscope was equipped with an energy-dispersive X-ray spectroscopy (EDX) system (Oxford Instruments) for compositional analysis. High-resolution transmission electron microscopy (HR-TEM) images were performed using an FEI Tecnai 30 microscope and a 20 microscope, operating at accelerating voltage of 300 kV and 200 kV, respectively. The scanning transmission electron microscopy (STEM)-EDX line scans analysis was performed in FEI TITAN 80-300 electron microscope (300 kV) equipped with an image corrector (CEOS) and a high-angle annular dark-field (HAADF) detector. Fourier transform infrared spectroscopy (FTIR) data were obtained using a Bruker Tensor 27 FTIR spectrometer. The X-ray photoelectron spectroscopy (XPS) measurements were conducted using an Omicron XPS system with Al Kα X-rays as the extinction source, operating at a voltage of 15 kV and a power of 300 W. Raman analysis was done with a confocal Raman microscope (CRM) (Alpha300R, WITec GmbH, Germany) equipped with a TEM single-frequency laser (λ=532 nm, laser power = 40 mW, WITec GmbH, Germany). The BET surface area was measured using nitrogen adsorption at 77 K and conducted on an ASAP 2020 instrument. Before the measurement, a 100 mg sample was preheated at 120 °C for 3 h to ensure degassing. All the electrochemical tests were performed using the IviumState2.h electrochemical workstation.

1.4. Electrochemical Measurements

Electrochemical measurements were performed using the IviumState2.h electrochemical workstation. To prepare the working electrode, a specific amount of catalyst (5 mg) was dispersed in a 950 µL mixed solvent of H_2O and EtOH (1:1, v/v) along with 50 µL of Nafion (5 wt.%). The mixture was sonicated for 30 min to obtain a colloidal suspension, and then 50 µL of the suspension ink (~0.25 mg catalyst) was dispersed on the substrate (NF or carbon paper, 1 x 1 cm) and allowed to air dry (~2 h at 20-25 °C). A standard three-electrode system was employed for electrochemical measurement,

as-prepared working electrode, Hg/HgO or an Ag/AgCl (KCl-saturated) served as the reference electrode, and a graphite-rod or Pt-wire was chosen as the counter electrode in 1 M KOH alkaline or 0.5 M H_2SO_4 acidic electrolyte, respectively. All the potentials were converted to the reversible hydrogen electrode (RHE) according to the Nernst equation, $E_{(RHE)} = E_{(Hg/HgO)} + 0.059pH + 0.098$ in alkaline electrolyte and $E_{(RHE)} = E_{(Ag/AgCl)} + 0.059pH + 0.197$ in acidic electrolyte. All the data have been corrected for a 90% IR potential drop. Polarization curves were recorded by linear sweep voltammetry (LSV) test at a scan rate of 5 mV/s. The current density was obtained by normalizing the current to the geometric surface area of the working electrode.

1.4.1. Synthesis of 20% Pt/C Electrode

To prepare 20% Pt/C electrode, a 5 mg catalyst was dispersed in a 950 µL mixed solution of H_2O and EtOH (1:1, v/v) along with 50 µL of Nafion (5 wt.%). The mixture was sonicated for 30 min to obtain a colloidal suspension, and then 50 µL of the suspension ink was dispersed on a substrate (carbon paper or NF, 1 x 1 cm) and allowed to air dry (~2 h at 20-25 °C).

1.4.2. Electrochemical Impedance Spectroscopy (EIS)

The EIS test was conducted using the AC impedance method over a frequency range of 0.01 to 1000 kHz with a 5 mV amplitude in different electrolyte solutions (i.e., 1 M KOH alkaline, 1 M KOH alkaline in seawater, 1 M PBS electrolyte, and 0.5 M H_2SO_4 acidic). The electrochemical parameters were extracted and analyzed by fitting the EIS data using ZView4 software.

1.4.3. Electrochemical Surface Area (ECSA)

The ECSA is determined using the formula $ECSA = C_{dl}/Cs$, where C_{dl} is the double-layered capacitance, and Cs is the specific capacitance, taken as 40 µF/cm^2. To estimate C_{dl}, CV was recorded within the non-faradaic potential region, specifically from 0 to -0.2 V vs RHE in 1 M KOH alkaline or 0.5 M H_2SO_4 acidic electrolytes. The roughness factor (R_f) was calculated by dividing ECSA by 0.08 cm^2, the geometric area of the electrode.

1.4.4. Stability Test, Chronopotentiometry (CP), and Chronoamperometry (CA)

The dynamic stability was assessed over 5000 CV cycles at a constant scan rate of 100 mV/s. After completing the 5000 CV cycles, a polarization curve was recorded to compare with the initial curve. The CP test was performed in different electrolyte solutions (i.e., 1 M KOH alkaline, 1 M KOH alkaline in seawater, 1 M PBS electrolyte, and 0.5 M H_2SO_4 acidic) at varying potentials to evaluate the catalyst stability. The CA test was conducted at potentials of -150 mV vs RHE in different electrolyte solutions (i.e., 1 M KOH alkaline, 1 M KOH alkaline in seawater, 1 M PBS electrolyte, and 0.5 M H_2SO_4 acidic) to assess the stability further.

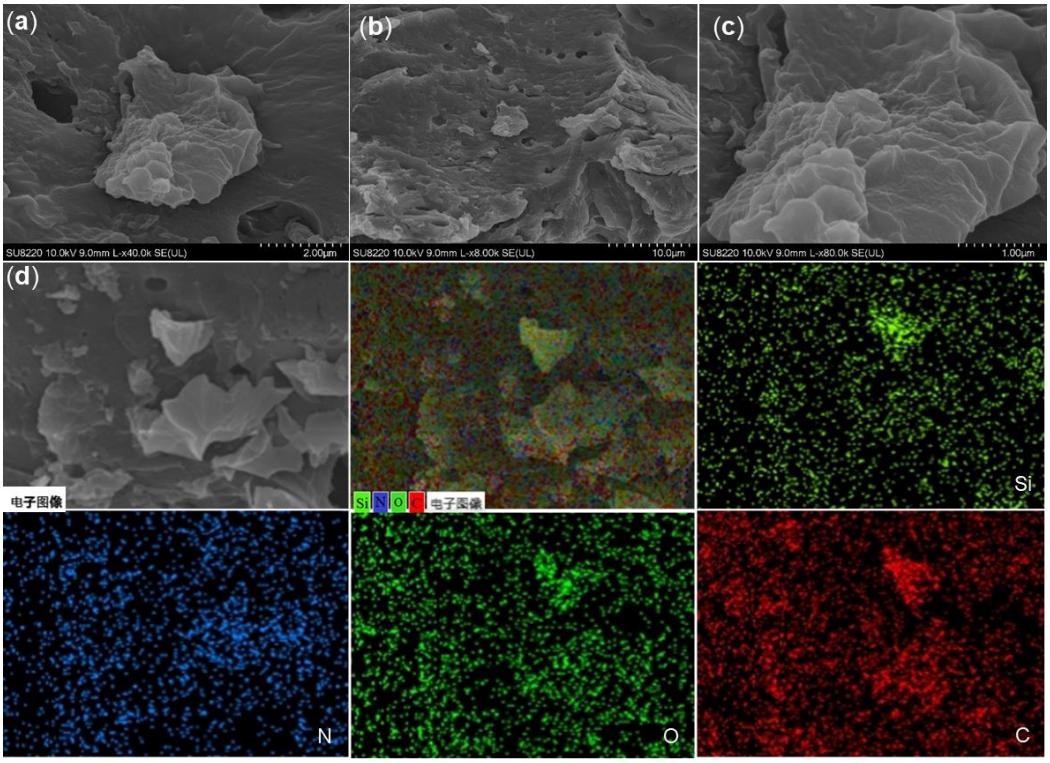

Fig. S2 (**a-c**) SEM images of OAPS-GMA with different magnifications and (**d**) EDS elemental mapping of Si, N, O, and C in OAPS-GMA.

Description: The SEM analysis depicts the surface morphology of OAPS-GMA at different magnifications. The results show that the surface appears relatively smooth with some wrinkled textures, suggesting the informality of the as-synthesized OAPS-GMA dendrimer. This kind of morphology is often seen in dendrimer or polymeric materials due to their branched, complex architecture. The EDS mapping confirms the presence of Si, O, N, and C in the OAPS-GMA dendrimer structure.

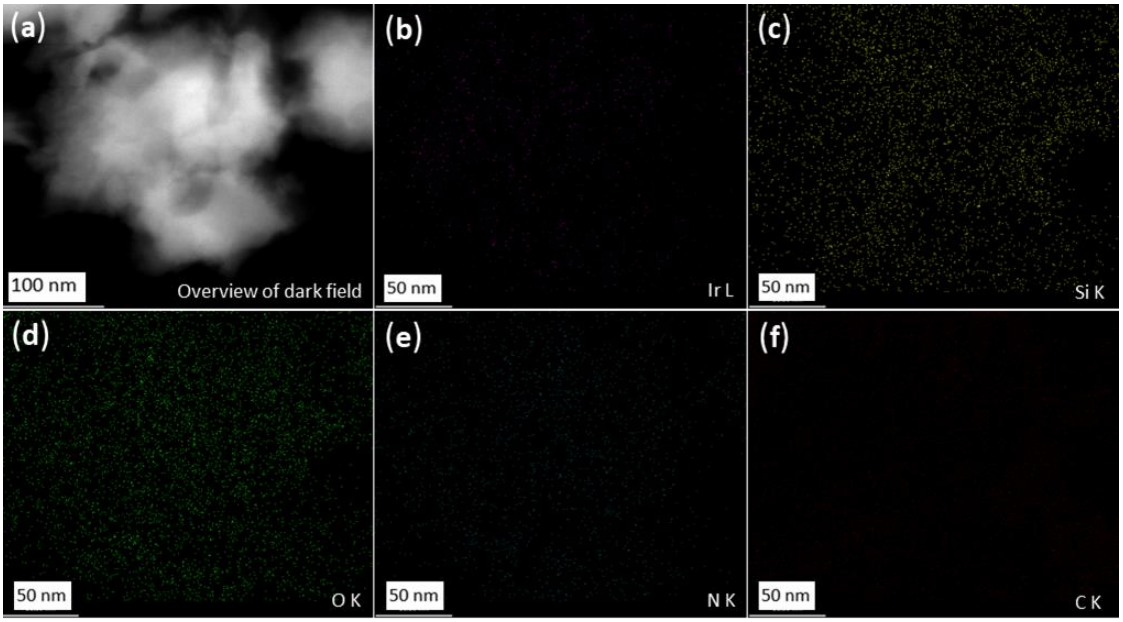

Fig. S3 The STEM-EDS elemental mapping of **Ir-OAPS-GMA**: (**a**) Overview of dark field, (**b**) Ir, (**c**) Si, (**d**) O, (**e**) N, and (**f**) C.

Discussion: The STEM-EDS elemental mapping observation confirms that the Ir is uniformly distributed in the OAPS-GMA core structure. Meanwhile, the elemental mappings of Si, O, N, and C show uniform distributions, consistent with their role in forming the OAPS-GMA dendrimer framework, which constituents the core-shell dendrimer structure.

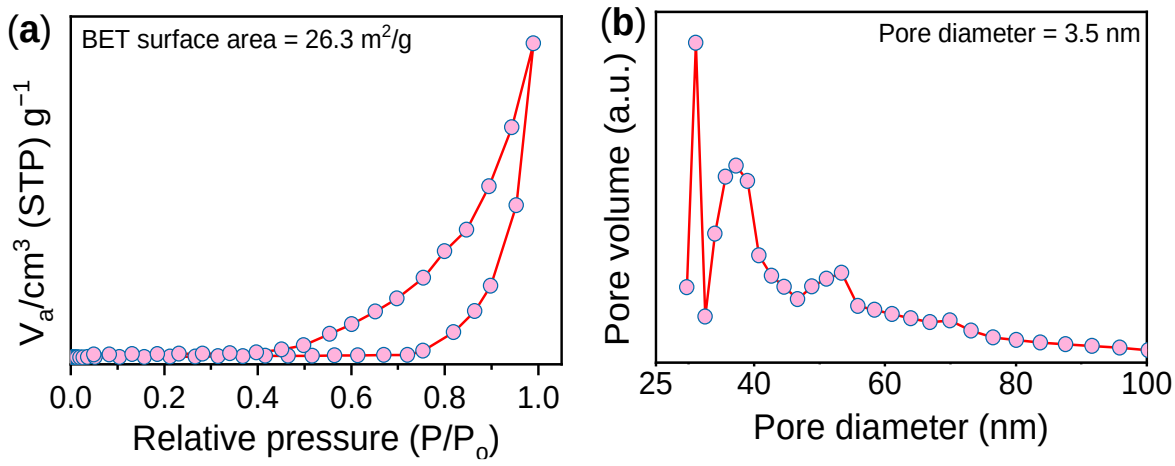

Fig. S4 (**a**) N_2 adsorption/desorption isotherm and (**b**) BJH pore-size distribution of **Ir-OAPS-GMA**.

Description: Nitrogen adsorption/desorption isotherms analysis was used to study the surface area of **Ir-OAPS-GMA**. The mid-to-high pressure range of the hysteresis loop indicates that the **Ir-OAPS-GMA** belongs to the type-IV isotherm. The **Ir-OAPS-GMA** exhibited a BET surface area of 26.3 m^2/g with a BJH pore-size distribution of 3.5 nm.

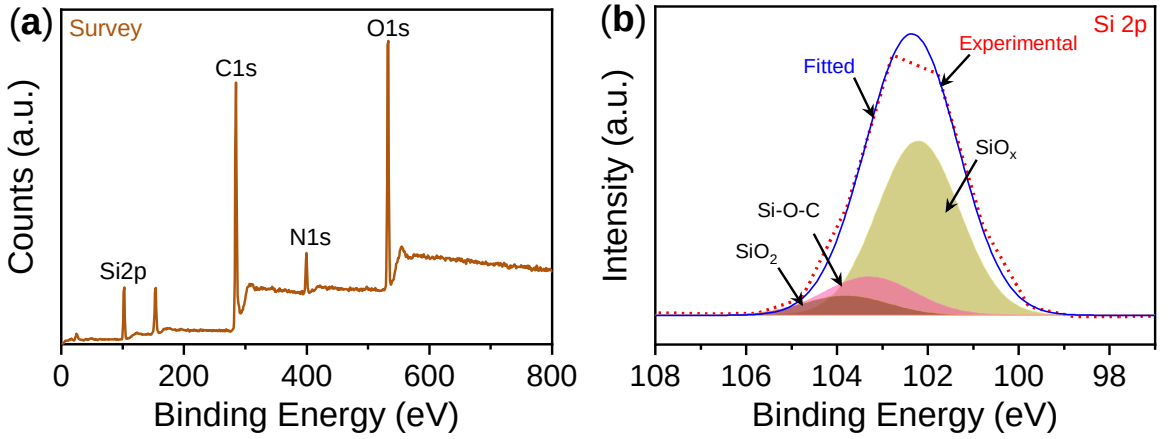

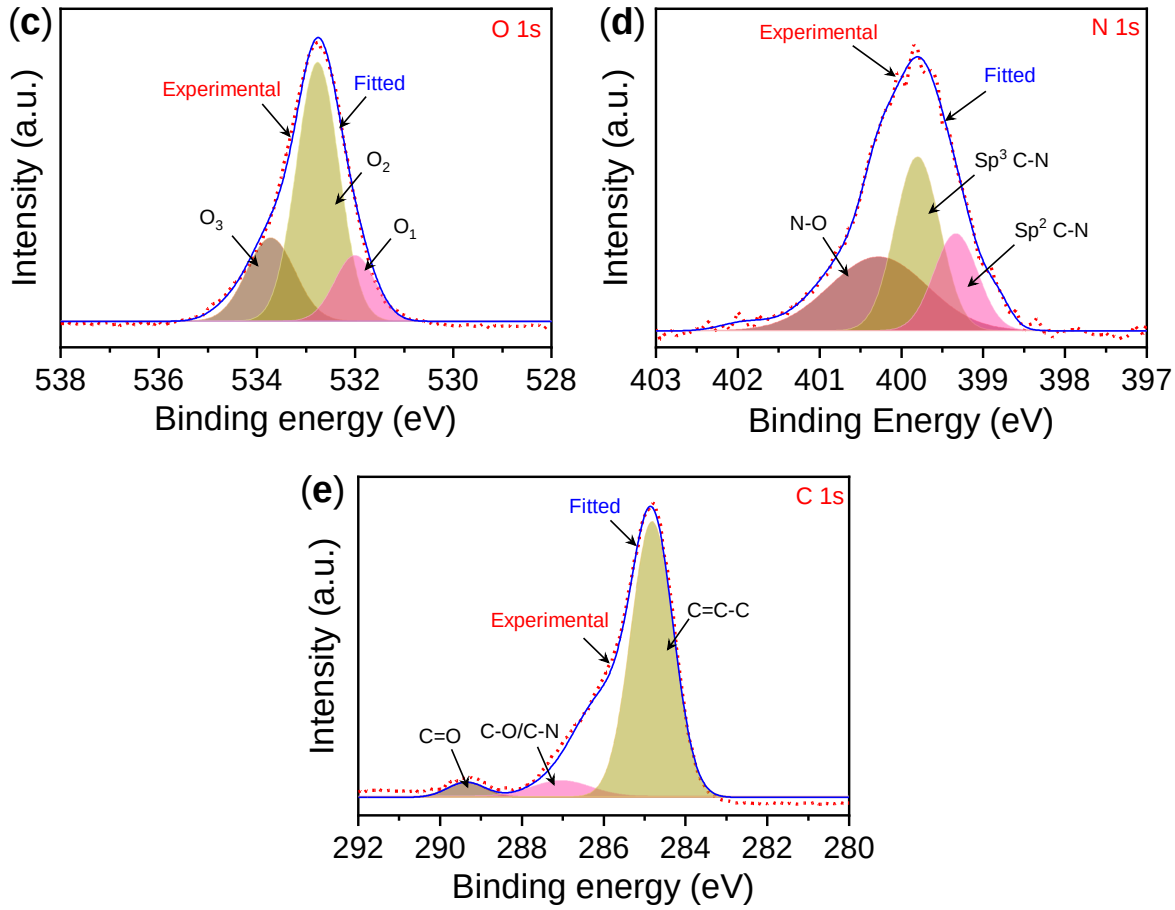

Fig. S5 XPS spectra of OAPS-GMA: (**a**) Survey spectrum, (**b**) Si 2p, (**c**) O 1s, (**d**) N 1s, and (**e**) C 1s.

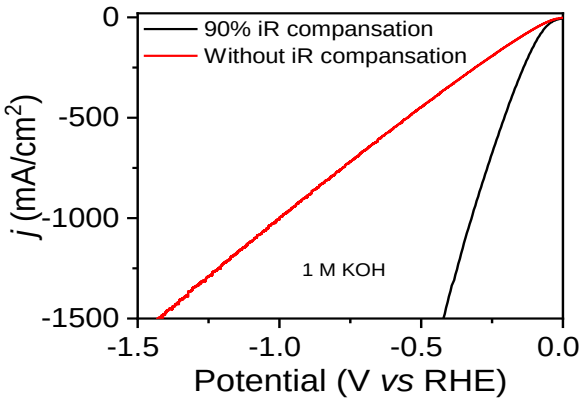

Fig. S6 LSV polarization curves of **Ir-OAPS-GMA** with 90% iR compensation and without iR compensation in electrochemical HER using 1 M KOH.

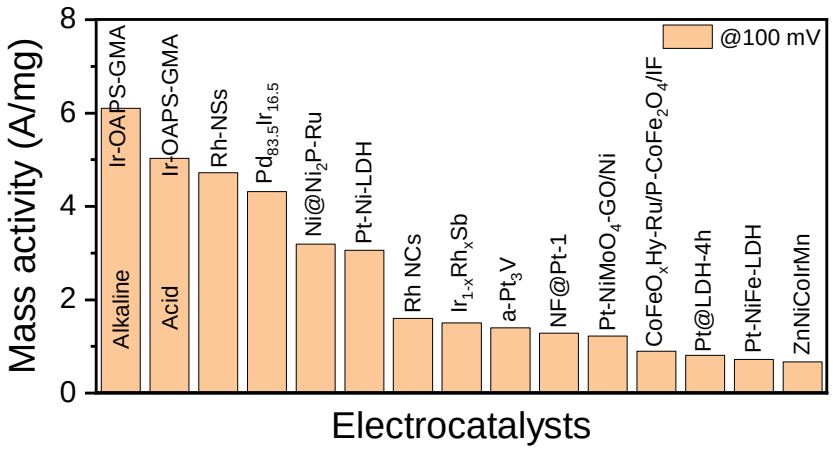

Fig. S7 Mass activity comparison chart of **Ir-OAPS-GMA** in both alkaline and acidic electrolytes with other state-of-the-art noble metal electrocatalysts in various electrolytes.

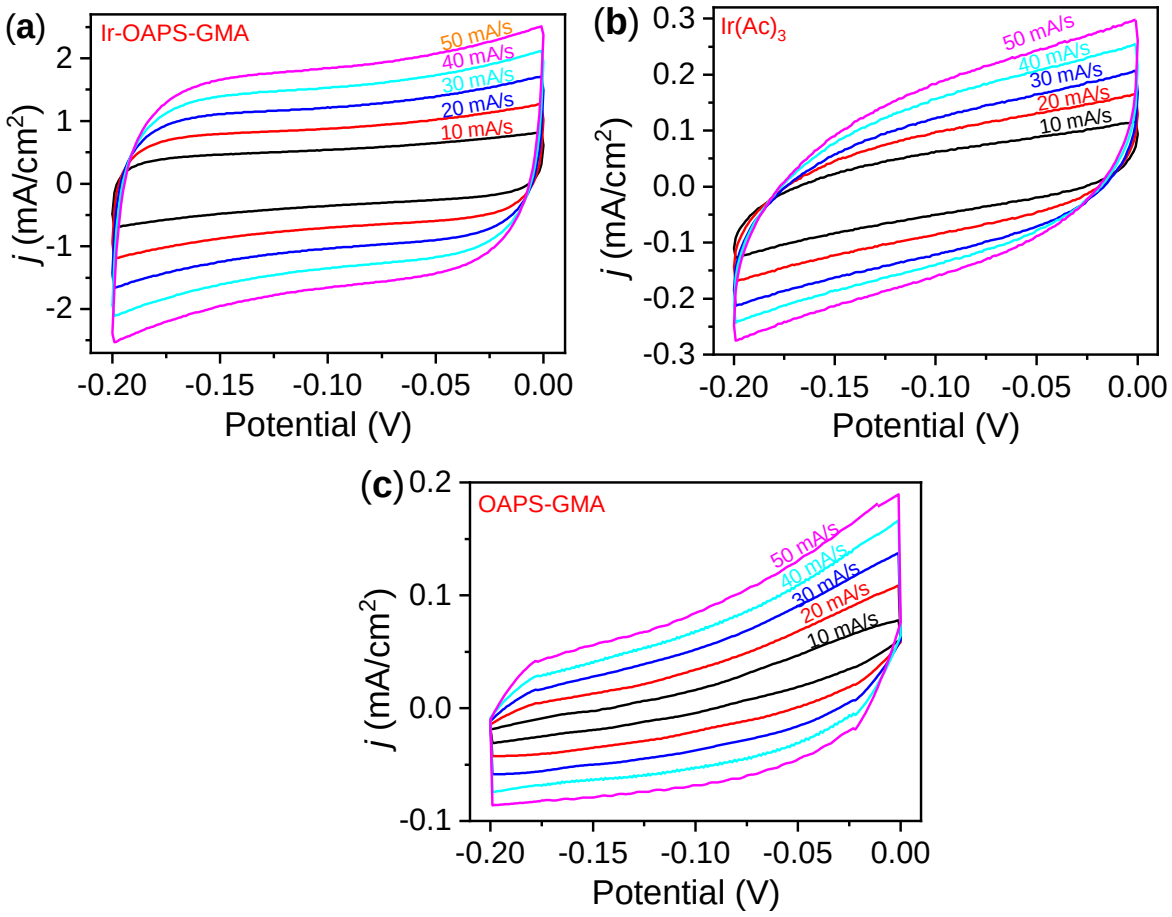

Fig. S8 Double-layered capacitance (C_{dl}) was measured in 1 M KOH electrolyte to determine the ECSA and roughness factor (RF) for HER. (**a**) **Ir-OAPS-GMA**, (**b**) $Ir(Ac)_3$, and (**c**) OAPS-GMA.

Description: The electrochemical surface area (ECSA) measurement was determined using the formula ECSA = C_{dl}/Cs, where C_{dl} is the double-layered capacitance, and Cs is the specific capacitance. The cyclic voltammetry was recorded within the non-faradaic potential region (i.e., 0 to -0.2 V vs. RHE) in a 1 M KOH alkaline electrolyte. The value of C_{dl} for **Ir-OAPS-GMA** = 32.43 mF/cm^2, $Ir(Ac)_3$ = 5.66

mF/cm^2, and OAPS-GMA = 3.52 mF/cm^2. The roughness factor (RF) values for **Ir-OAPS-GMA**, Ir(Ac)$_3$, and OAPS-GMA are 810.75, 141.5, and 88.0, respectively.

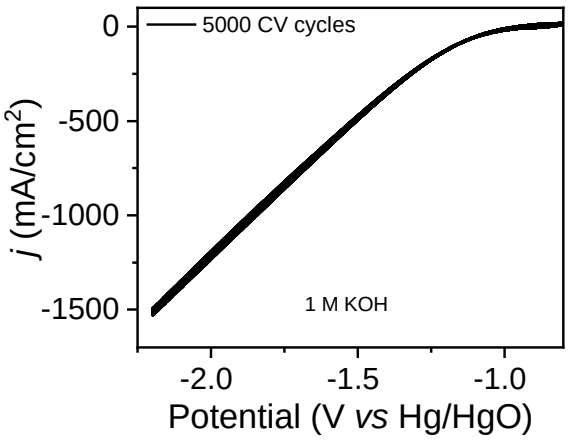

Fig. S9 Cyclic voltammetry 5000 cycles for the stability of **Ir-OAPS-GMA** in electrochemical HER using 1 M KOH electrolyte.

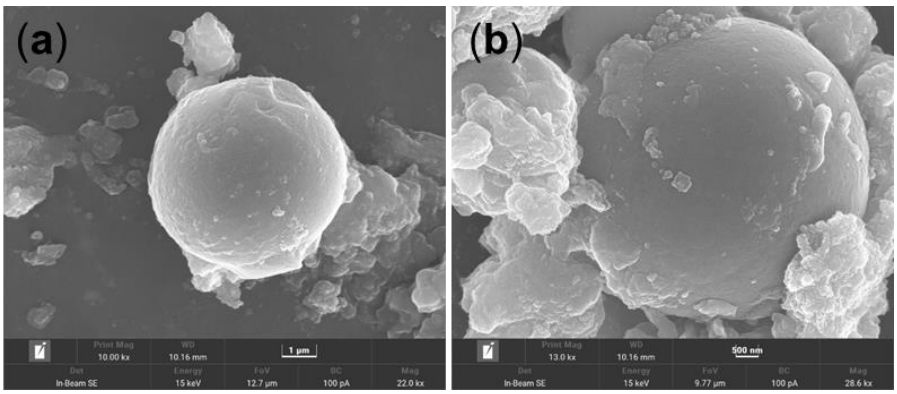

Fig. S10 SEM image of **Ir-OAPS-GMA** at different magnifications after electrochemical HER in 1 M KOH electrolyte.

Description: The structural stability of **Ir-OAPS-GMA** after the long-term HER testing in 1 M KOH electrolyte was studied by using SEM analysis. The SEM images reveal that the **Ir-OAPS-GMA** maintains its spherical morphology with slight changes on its surface. The results signify the **Ir-OAPS-GMA** high structural integrity. The comprehensive stability evaluation demonstrates the potential of **Ir-OAPS-GMA** as a highly effective and durable electrocatalyst for hydrogen production in practical applications.

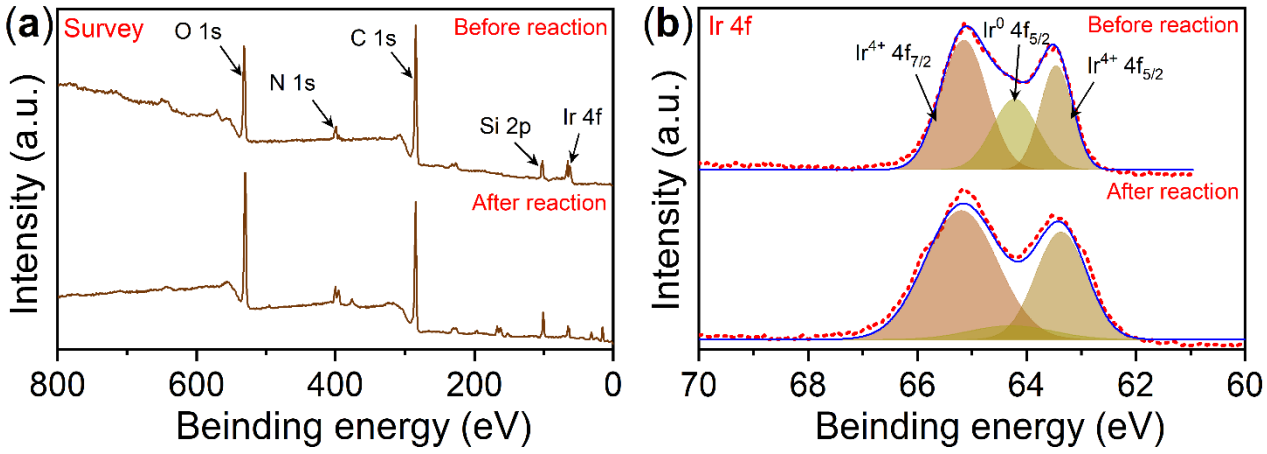

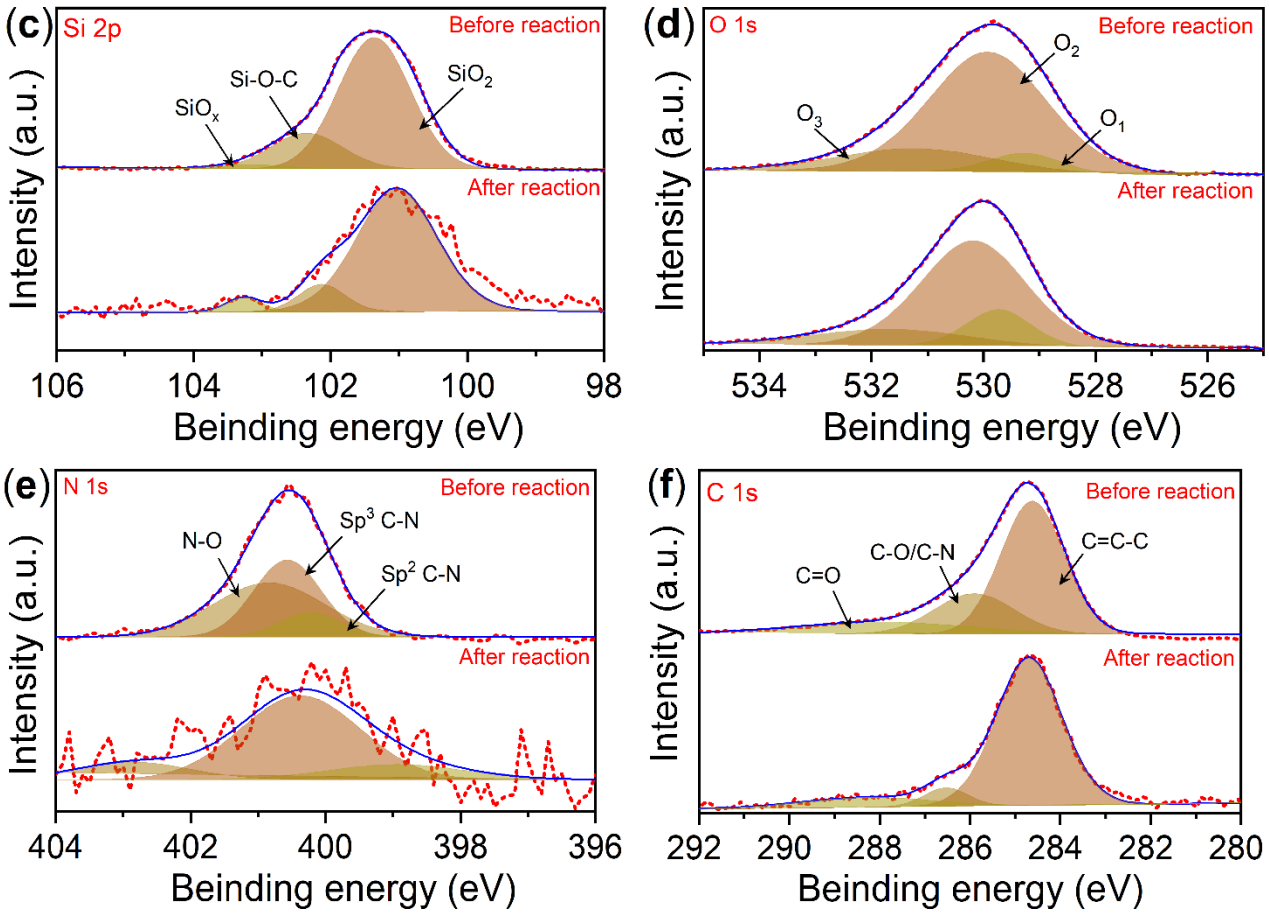

Fig. S11 XPS spectra of **Ir-OAPS-GMA** before and after electrochemical HER in 1 M KOH electrolyte: (a) Survey spectrum, (b) Ir 4f, (c) Si 2p, (d) O 1s, (e) N 1s, and (f) C 1s.

Description: XPS analysis was carried out to further evaluate the stability of **Ir-OAPS-GMA** after the long-term HER testing in 1 M KOH electrolyte. After the long-term HER test, the results indicate some noise in the Si 2p and N 1s spectrum. However, the XPS analysis confirms that there are no significant changes in the elemental composition or chemical valance of Ir 4f, Si 2p, O 1s, N 1s, and C 1s, thereby strengthening the stability of the material during the electrochemical HER.

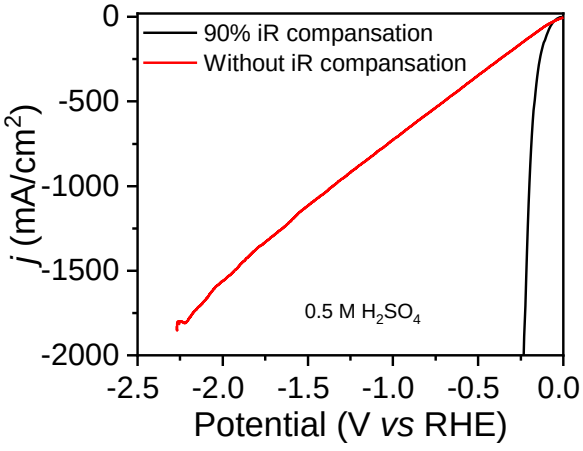

Fig. S12 LSV polarization curves of **Ir-OAPS-GMA** with 90% iR compensation and without iR compensation in electrochemical HER using 0.5 M H_2SO_4.

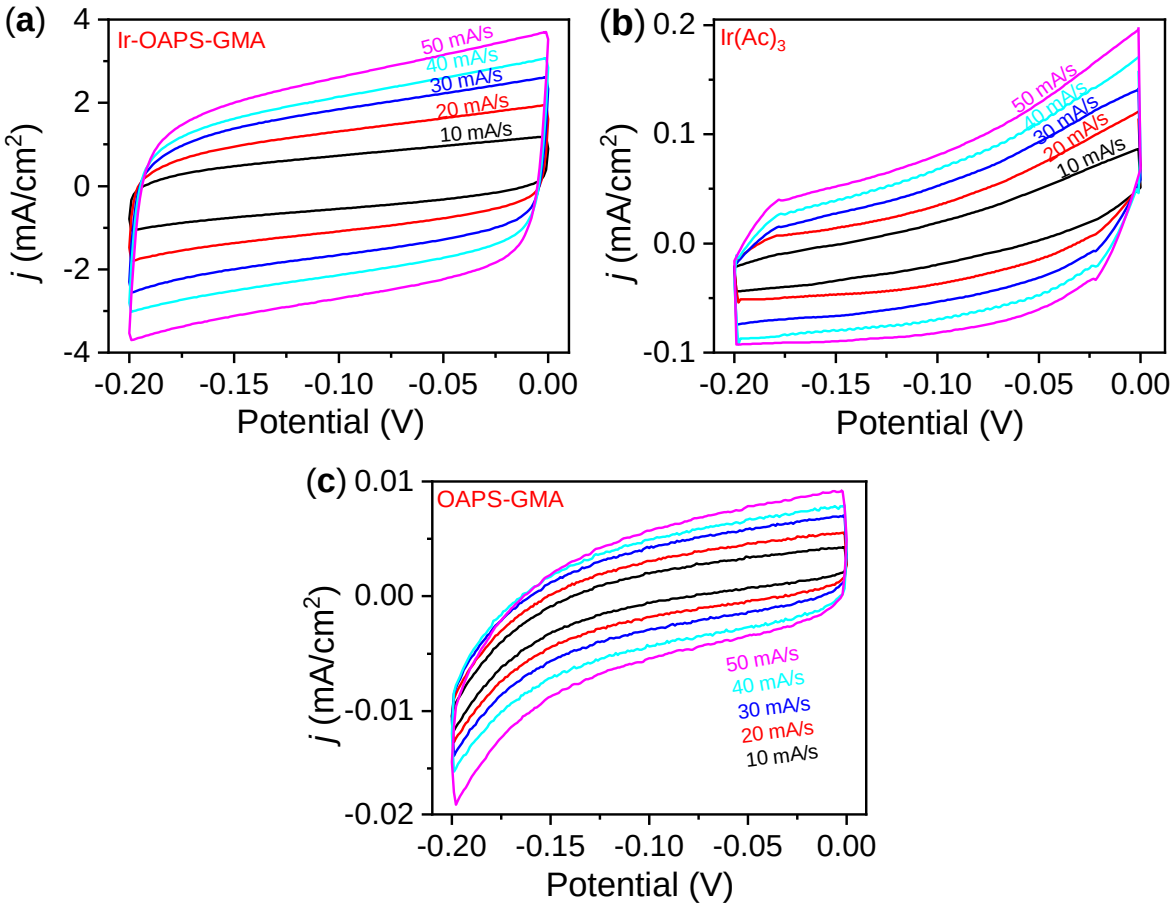

Fig. S13 Double-layered capacitance (C_{dl}) was measured in 0.5 M H_2SO_4 electrolyte to determine the ECSA and roughness factor (RF) for HER. (**a**) **Ir-OAPS-GMA**, (**b**) $Ir(Ac)_3$, and (**c**) OAPS-GMA.

Description: The cyclic voltammetry was recorded within the non-faradaic potential region (i.e., 0 to -0.2 V vs RHE) in a 0.5 M H_2SO_4 acidic electrolyte. The value of C_{dl} for **Ir-OAPS-GMA** = 46.9 mF/cm^2, $Ir(Ac)_3$ = 2.8 mF/cm^2, and OAPS-GMA = 1.2 mF/cm^2. The roughness factor (RF) values for **Ir-OAPS-GMA**, $Ir(Ac)_3$, and OAPS-GMA are 1172.5, 70.0, and 30.0, respectively.

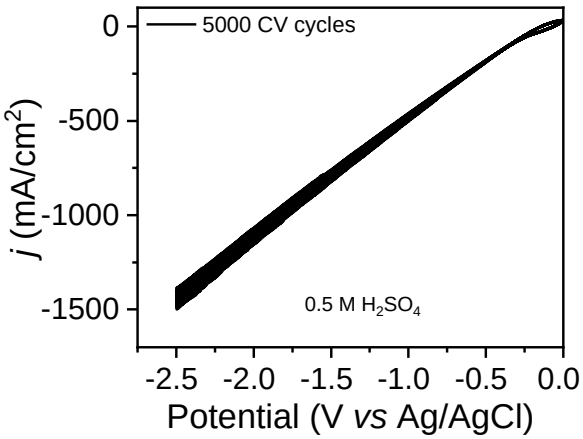

Fig. S14 Cyclic voltammetry 5000 cycles for the stability of **Ir-OAPS-GMA** in electrochemical HER using 0.5 M H_2SO_4 electrolyte.

Table S1. Mass activity, intrinsic catalytic activities, and cost-effectiveness comparison of **Ir-OAPS-GMA** with other reported state-of-the-art noble metal electrocatalysts in various electrolytes.

Catalysts and Experimental Setup					Performance Metrics			Economics Analysis		
Catalysts	Electrolyte	Catalyst load (μg)	Overpotential (mV)	Current density (mA/cm^2)	Tafel slope (mV/dec)	Long term stability (h)	Total current density (mA/cm^2)	Mass activity (noble metal contents in A/mg)	Estimated cost based on noble metals	Ref.
Ir-OAPS-GMA	1 M KOH	22.5 μg_{Ir} /cm^2	18.8	10	67.6	340 h	1500	6.10 A/mg_{Ir}@100 mV	1 time	This study
Ir-OAPS-GMA	0.5 M H_2SO_4	22.5 μg_{Ir} /cm^2	35	10	29.6	340 h	1500	5.03 A/mg_{Ir}@100 mV	1 time	This study
Pt@LDH-4h	1 M KOH	89.2 μg_{Pt} /cm^2	58.7	10	43.6	24 h	710	0.81 A/mg_{Pt}@100 mV	2.27 time based on Pt	*Small* 2023, **19**, 2207044.
Pt-$NiMoO_4$-GO/Ni	1 M KOH	57 μg_{Pt} /cm^2	94	10	81.4	48 h	250	1.22 A/mg_{Pt}@100 mV	1.45 time based on Pt	J. Colloid Interface Sci. 2023, **640**, 928-939.
Rh-NSs	1 M KOH	55 μg_{Rh} /cm^2	42	10	30	1.6 h	720	4.72 A/mg_{Rh}@100 mV	10.38 time based on Rh	*Nanoscale* 2019, **11**, 9319-9326.
Pt-NiFe-LDH	1 M KOH	1880 μg_{Pt} /cm^2	36	10	50	120 h	300	0.72 A/mg_{Pt}@100 mV	48.04 time based on Pt	Appl. Catal. B: Environ. 2023, **331**, 122683.
$Ir_{1-x}Rh_xSb$	0.5 M H_2SO_4	66 μg_{Ir} /cm^2	200	10	47.6	55 h	200	1.50 A/mg_{Ir}@100 mV	2.93 time based on Ir	Adv. Energy Mater. 2022, **12**, 2200855
$CoFeO_xHy$-Ru/P-$CoFe_2O_4$/If	1 M KOH	311 μg_{Ru} /cm^2	38	50	43.2	38 h	200	0.90 A/mg_{Ru}@100 mV	11.40 time based on Ru	Inorg. Chem. Front. 2022, **9**, 1847-1855.
NF@Pt-1	0.5 M H_2SO_4	1300 μg_{Pt} /cm^2	54.3	10	54.3	48 h	48	1.28 A/mg_{Pt}@100 mV	33.22 time based on Pt	*J. Power Sources* 2023, **579**, 233262.
ZnNiCoIrMn	0.1 M $HClO_4$	112.4 μg_{Ir} /cm^2	55	50	36.6	100 h	980	0.67 A/mg_{Ir}@100 mV	4.99 time based on Ir	*Adv. Mater.* 2023, **35**, 2300091.
Ni@Ni_2P-Ru	0.5 M H_2SO_4	263.2 μg_{Ru} /cm^2	51	10	35	11.1 h	70	3.19 A/mg_{Ru}@50 mV	9.65 time based on Ru	*J. Am. Chem. Soc.* 2018, **140**, 2731-2734.

Pt-Ni-LDH	1 M KOH	150 μg_{Pt} /cm^2	52	10	46	120 h	100	3.06 A/mg_{Pt}@100 mV	3.83 time based on Pt	Adv. Funct. Mater. 2024, **34**, 2308575.
Rh NCs	0.1 M $HClO_4$	42 μg_{Rh} /cm^2	64	10	107	5 h	196	1.60 A/mg_{Rh}@100 mV	7.93 time based on Rh	*Chem. Mater.* 2017, **29**, 5009-5015.
$Pd_{83.5}Ir_{16.5}$	0.5 M H_2SO_4	243 μg_{Pd} /cm^2	73	10	43.6	60 h	560	4.32 A/mg_{Ir}@100 mV	10.80 time based on Pd	*Inorg. Chem.* 2020, **59**, 3321-3329.
a-Pt_3V	0.5 M H_2SO_4	64 μg_{Pt} /cm^2	20	10	36	100 h	1000	1.50 A/mg_{Pt}@100 mV	2.34 time based on Pt	Adv. Energy Mater. 2023, **13**, 2300127.

Discussion: The table provides a clear comparison of the catalytic performance and cost-effectiveness of **Ir-OAPS-GMA** with state-of-the-art noble metal-based electrocatalysts for HER. In the table, the catalyst loadings reflect the amount of noble metal deposited on the electrode, with values either directly sourced from the literature or calculated based on the reported composition. The catalytic performance matrices, including overpotential, current density, Tafel slope, stability, and mass activity, were collected from the experimental results or graphs in the reported studies, ensuring fair comparison. The estimated costs are calculated relative to noble metal loading, using **Ir-OAPS-GMA** as the standard (1x cost), allowing for fair economic comparisons. All the data were collected from the reported literature with adjustment made for consistency. The high mass activity, long-term stability, and cost-effectiveness of the **Ir-OAPS-GMA** make it a strong candidate for practical HER production applications.

Table S2. Comparison of **Ir-OAPS-GMA** with other reported Ir-based electrocatalysts for HER in alkaline electrolyte.

Catalysts type	Electrolyte	Catalyst load	Overpotential (mV)	Current density	Tafel slope (mV/dec)	Stability	References
Ir-OAPS-GMA	*1 M KOH*	*0.25 mg*	*18.86*	*10 mA/cm²*	*67.6*	*340 h*	*This work*
Ir-OAPS-GMA	*1 M KOH*	-	*61.41*	*50 mA/cm²*	-	-	*This work*
Ir-OAPS-GMA	*1 M KOH*	-	*85.52*	*100 mA/cm²*	-	-	*This work*
Co@Ir/NC-10%	1 M KOH	0.202 mg	121	10 mA/cm²	38	12 h	Li et al., *ACS Sustain. Chem. Eng.* 2018, **6**, 5105-5114.
Ir/MoS_2	1 M KOH	0.285 mg	41	10 mA/cm²	32	18 h	Wei et al., *ACS Energy Lett.* 2018, **4**, 368-374.
PdIr UNWs/WFG	1 M KOH	0.04 mg	23	10 mA/cm²	38.4	24 h	Yang et al., *Nanoscale* 2019, **11**, 14561-145.
Co-Ir-600	1 M KOH	0.89 mg	85	10 mA/cm²	46.7	20 h	W. Li et al., *Sci. China Mater.* 2023, **66**, 1024-1032.
Ir/VC/C-100	1 M KOH	0.0667 mg	22	10 mA/cm²	45.2	10 h	Li. Wu et al., *Chem. Commun.* 2021, **57**, 10395-10398.
D-$IrTe_2$ HNSs	1 M KOH	4 μg	54	10 mA/cm²	32.7	2.8 h	Pi et al., *Adv. Funct. Mater.* 2020, **30**, 2004375.
3% IrO_2@BCNT	1 M KOH	0.28 mg	56	10 mA/cm²	20	20 h	Liu et al. *J. Chem. Eng.* 2021, **419**, 129567.
RuIr@NRC	1 M KOH	0.464 mg	28	10 mA/cm²	35	30 h	Yu et al., *J. Chem. Eng.* 2021, **417**, 12810.
Ir_1@Co/NC	1 M KOH	0.163 mg	55	10 mA/cm²	119	5 h	Lai et al., *Angew. Chem., Int. Ed. Engl.* 2019, **58**, 11868-11873.
IrCo@NC-500	1 M KOH	0.2 mg	45	10 mA/cm²	80	-	Jiang et al., *Adv. Mater.* 2018, **30**, 1705324.
Ir/$NiPS_3$	1 M KOH	0.0769 mg/ 0.0192 mg CB	23	10 mA/cm²	35.8	25 h	Liu et al., *Nat. Commun.* 2024, **15**, 2851.
PtIr/IrOx-30 NWs/C	1 M KOH	15 μg	20	10 mA/cm²	38	10 h	Huang et al., *Small* 2022, **18**, 2201333.
Ir-g-CN	1 M KOH	0.119 mg	60.2	10 mA/cm²	47.6	120 h	Yu et al., *Appl. Catal. B: Environ.* 2022, **310**, 121318.

$Ir_{1-x}Rh_xSb$	1 M KOH	0.06 mg	200	10 mA/cm^2	47.6	55 h	Lin et al., *Adv. Energy Mater.* 2022, **12**, 2200855.
IrP_2@NC	1 M KOH	0.7 mg	28	10 mA/cm^2	28	10 h	Pu et al., *Energy Environ. Sci.* 2019, **12**, 952-957.
$PtIr_{0.05}$-$Co_2P/Co_2P_2O_7$ NWs/C	1 M KOH	-	63	10 mA/cm^2	69	50 h	Austeria et al., *Appl. Catal. B: Environ.* 2023, **327**, 122467.
IrO_2-RuO_2/C	1 M KOH	0.025 mg	75	10 mA/cm^2	52	24 h	Samanta et al., *Energy Fuels* 2022, **36**, 1015-1026.
$Ir_{0.80}Ru_{0.20}O_y$	1 M KOH	0.06 mg	34	10 mA/cm^2	31.5	2.8 h	Cho et al., *ACS Appl. Mater. Interfaces* 2018, **10**, 541-549.
IrNi-$FeNi_3$/NF	1 M KOH	-	32.1	10 mA/cm^2	66.9	120 h	Wang et al., Appl. Catal. B: Environ. 2021, **286**, 119881.
Ir@Ni/NiO	1 M KOH	3.8 mg	190	10 mA/cm^2	115.6	30 h	D. Li et al., *Appl. Energy* 2024, **356**, 122369.
Ir/C/Ni/NiO	1 M KOH	3.8 mg	5540	10 mA/cm^2	71	-	D. Li et al., *Appl. Energy* 2024, **356**, 122369.
Ir-NiCo LDH	1 M KOH	2 mg	33.2	10 mA/cm^2	34.3	2 h	Fan et al., *J. Mater. Chem. A* 2020, **8**, 9871-9881.

Table S3. Comparison of **Ir-OAPS-GMA** with other reported Ir-based electrocatalysts for HER in acidic electrolyte.

Catalysts type	**Electrolyte**	**Catalyst load**	**Overpotential (mV)**	**Current density**	**Tafel slope (mV/dec)**	**Stability**	**References**
Ir-OAPS-GMA	*0.5 M H_2SO_4*	*0.25 mg*	35	*10 mA/cm^2*	*29.6*	*340 h*	*This work*
Ir-OAPS-GMA	0.5 M H_2SO_4	-	71	10 mA/cm^2	-	-	*This work*
Ir-OAPS-GMA	0.5 M H_2SO_4	-	95	10 mA/cm^2	-	-	*This work*
Ir/WO_x/rGO	0.5 M H_2SO_4	0.095 mg	53	10 mA/cm^2	83	-	Huang et al., *J. Mater. Sci.* 2020, **55**, 5554-5570.
IrCoNi	0.1 M $HClO_4$	10 μg Ir	33	10 mA/cm^2	31.9	3.3 h	Feng et al., *Adv. Mater.* 2017, **29**, 1703798.
CB[6]-Ir_2	0.5 M H_2SO_4	20 μg Ir	54	10 mA/cm^2	51	12 h	You et al., *ACS Energy Lett.* 2019, **4**, 1301-1307.

Ir nanorods	0.5 M H_2SO_4	0.283 mg	31	10 mA/cm^2	72	12 h	Luo et al., *Appl. Catal. B: Environ.* 2020, **279**, 119394.
Ru-P (Ir at. 3%)	0.5 M H_2SO_4	0.2 mg	33	10 mA/cm^2	33	24 h	Jung et al., *Adv. Fiber Mater.* 2024, **6**, 158-169.
IrO_2-Fe_2O_3	0.5 M H_2SO_4	0.125 mg	78	10 mA/cm^2	36.2	600 CV cycles	Yang et al., *RSC Adv.* 2017, **7**, 20252-20258.
IrNiN NPs	0.1 M $HClO_4$	0.015 mg	110	10 mA/cm^2	36	-	Kuttiyiel et al., *J. Mater. Chem. A,* 2014, **2**, 591-594.
IrO_2-TiO_2	0.5 M H_2SO_4	0.25 mg	112	10 mA/cm^2	46.8	18 h	Yuan et al., *New J. Chem.* 2017, **41**, 6152-6159.
IrNiTa/Si	0.5 M H_2SO_4	8.1 μg Ir	99	10 mA/cm^2	35	10 h	Z. J. Wang et al., *Adv. Mater.* 2020, **32**, 1906384.
Ir-NCNSs	0.5 M H_2SO_4	0.254 mg	52	10 mA/cm^2	52	10 h	X. Wu et al., *ACS Appl. Mater. Interfaces.* 2021, **13**, 22448-22456.
Ir/Si	0.5 M H_2SO_4	24.9 μg Ir	59	10 mA/cm^2	20	1000 CV cycles	Z. J. Wang et al., *Adv. Mater.* 2020, **32**, 1906384.
IrCo@NC-500	0.5 M H_2SO_4	0.2 mg	24	10 mA/cm^2	23	2.8 h	Jiang et al., *Adv. Mater.* 2018, **30**, 1705324.
Ir NPs/silene	0.5 M H_2SO_4	0.283 mg	31	10 mA/cm^2	29.4	8 h	Dai et al., *Chem. Commun.* 2020, **56**, 4824-4827.
Co@Ir/NC-10%	0.5 M H_2SO_4	0.202 mg	29.4	10 mA/cm^2	41.9	3000 CV cycles	Li et al., *ACS Sustain. Chem. Eng.* 2018, **6**, 5105-5114.
$Pd_{83.5}Ir_{16.5}$	0.5 M H_2SO_4	0.0199 μg	73	10 mA/cm^2	43.6	60 h	C. Wang et al., *Inorg. Chem.* 2020, **59**, 3321-3329.
IrRu NPs	0.1 M $HClO_4$	12 μg Ir	52	10 mA/cm^2	73	100 h	Joo et al., *J. Mater. Chem. A,* 2018, **6**, 16130-16138.
$Er_2Si_2O_7$:IrO_2	0.5 M H_2SO_4	15 mg	49	10 mA/cm^2	49	4.1 h	Karfa et al., *ACS Catal.* 2018, **8**, 8830-8843.
BPIr-be	0.5 M H_2SO_4	1.3 mg	1.54	10 mA/cm^2	30.9	15 h	Mei et al., *Adv. Mater.* 2021, **33**, 2104638.
Ir-doped WO_3	0.5 M H_2SO_4	0.5 mg	1.56	10 mA/cm^2	72	12 h	Li et al., *Small* 2021, **17**, 2102078.
Ir-Au-Si-2	0.5 M H_2SO_4	0.283 mg	38	10 mA/cm^2	24	15 h	Liao et al., *ChemCatChem* 2019, **11**, 2126-2130.

IrO_2-RuO_2/C	0.5 M H_2SO_4	0.025 mg	82	10 mA/cm^2	37	24 h	Samanta et al., *Energy & Fuels* 2022, **36**, 1015-1026.
IrCo@NC-850	0.5 M H_2SO_4	0.226 mg	50	10 mA/cm^2	64	2.8 h	Zhou et al., *Adv. Funct. Mater.* 2021, **31**, 2101797.
Ir@NG-750	0.5 M H_2SO_4	70 μg	19	10 mA/cm^2	26	20 h	Wu et al., *Nano Energy* 2019, **62**, 117-126.

Table S4. Comparison of **Ir-OAPS-GMA** with other reported Ir-based electrocatalysts for overall water splitting in alkaline electrolyte.

Catalysts type	**Electrolyte**	**Catalyst load**	**Overpotential (V)**	**Current density**	**Stability**	**References**
Ir-OAPS-GMA	*1 M KOH*	*0.25 mg*	*1.48*	*10 mA/cm^2*	*185 h*	*This work*
Ir-OAPS-GMA	*1 M KOH*	-	*1.586*	*50 mA/cm^2*	-	*This work*
Ir-NSs	*1 M KOH*	3 μg Ir	1.575	100 mA/cm^2	10 h	Cheng et al., *Natl. Sci. Rev.* 2020, **7**, 1340-1348.
Ir_3-$Ni(OH)_2$/NF	1 M KOH	-	1.54	10 mA/cm^2	12 h	Tong et al., *ChemCatChem* 2020, **12**, 5720-5726.
IrCo@NC	1 M KOH	0.226 mg	1.575	10 mA/cm^2	2.8 h	Zhou et al., *Adv. Funct. Mater.* 2021, **31**, 2101797.
IrW nanobranches	0.1 M KOH	0.06 mg	1.6	10 mA/cm^2	16.6	Fu et al., *Nanoscale* 2019, **11**, 8898-8905.
IrO-RuO_2/C	1 M KOH	0.025 mg	1.52	10 mA/cm^2	6 h	Samanta et al., *Energy Fuels* 2022, **36**, 1015-1026.
$IrVO_2$	1 M KOH	1 mg	1.54	10 mA/cm^2	12 h	Niu et al., *Adv. Mater.* 2024, **36**, 2310690.
Ir-NSG	1 M KOH	0.3 mg	1.6	10 mA/cm^2	24 h	Q. Wang et al., *at Commun.* 2020, **11**, 4246.
Ir-NR/C	1 M KOH	0.283 mg	1.57	10 mA/cm^2	12 h	Luo et al., *Appl. Catal. B* 2020, **279**, 119394.
Li-$IrSe_2$	1 M KOH	1 mg	1.5	10 mA/cm^2	24 h	Zheng et al., *Angew. Chem., Int. Ed. Engl.* 2019, **131**, 14906-14911.
IrO_2/V_2O_5	1 M KOH	0.1 mg Ir	1.49	10 mA/cm^2	30 h	Zheng et al., *Adv. Sci.* 2022, **9**, 2104636.
Ir-C≡	1 M KOH	1 mg Ir; 4 mg CB	1.495	10 mA/cm^2	20 h	Peng et al., *ACS Catal.* 2021, **11**, 1179-1188.

Pt-IrO_2/CC	1 M KOH	0.5 mg	1.492	10 mA/cm^2	50 h	Li et al., *Adv. Energy Mater.* 2020, **10**, 2001600.
Ir@Ni/NiO	1 M KOH	8 µg Ir	1.50	10 mA/cm^2	24 h	D. Li et al., *Appl. Energy* 2024, **356**, 122369.
Ir/CN	1 M KOH	0.497 mg	1.5	10 mA/cm^2	-	Wang et al., *ACS Appl. Mater. Interfaces* 2018, **10**, 22340-22347.
Ir/MoS_2	1 M KOH	0.285 mg	1.57	10 mA/cm^2	12 h	Wei et al., *ACS Energy Lett.* 2018, **4**, 368-374.
Ir_1@Co/NC	1 M KOH	0.163 mg	1.603	10 mA/cm^2	5 h	Lai et al., *Angew. Chem., Int. Ed. Engl.* 2019, **58**, 11868-11873.
FeIr/NF	1 M KOH	0.05 mg	1.48	10 mA/cm^2	500 h	Shen et al., *Appl. Catal. B: Environ.* 2020, **278**, 119327.
Ir/Ni_3Fe/rGO	1 M KOH	0.2 mg	1.574	10 mA/cm^2	24 h	Y. Li et al., *Chem. Eng. J.* 2023, **451**, 138548.
Fe-Co-Ni MOF	1 M KOH	1 mg	1.60	10 mA/cm^2	150 h	Shahbazi Farahani et al. *J. Am. Chem. Soc.* 2022, **144**, 3411-3428.
Ir-rEGO	1 M KOH	0.255	1.5	10 mA/cm^2	20 h	X. Li et al., *Adv. Funct. Mater.* 2024, 2313530.